OPEN ACCESS
IOP Publishing
Journal of Physics B: Atomic, Molecular and Optical Physics
J. Phys. B: At. Mol. Opt. Phys. **48** (2015) 175001 (8pp)
doi:10.1088/0953-4075/48/17/175001

Exciting positronium with a solid-state UV laser: the Doppler-broadened Lyman-α transition

A Deller[1,2], D Edwards[1], T Mortensen[1], C A Isaac[1], D P van der Werf[1], H H Telle[1,3] and M Charlton[1]

[1] Department of Physics, College of Science, Swansea University, Singleton Park, Swansea, SA2 8PP, UK
[2] Department of Physics and Astronomy, University College London, Gower Street, London, WC1E 6BT, UK
[3] Instituto Pluridisciplinar, Universidad Complutense, Paseo Juan XXIII-1, E-28040 Madrid, Spain

E-mail: a.deller@ucl.ac.uk

Received 21 March 2015, revised 18 May 2015
Accepted for publication 29 May 2015
Published 17 July 2015

Abstract

A tunable, pulsed laser was used to excite the Lyman-α transition (1S–2P) of positronium (Ps). The laser system has a large bandwidth of $\Delta\nu = 225$ GHz at $\lambda = 243$ nm, providing significant coverage of the Doppler-broadened, single-photon transition. The infra-red fundamental of a Nd:YAG laser was converted to ultraviolet by a series of solid-state, nonlinear processes, centred about an unseeded optical parametric oscillator, from which the bulk of the ultimate bandwidth derives. The Ps atoms were created by bombarding mesoporous silica with positrons, and the Doppler-width of the 1S–2P transition of the resulting ensemble was measured to be $\Delta\nu = 672 \pm 43$ GHz (equivalent to $T \approx 300$ K). It is envisaged that the UV laser will be incorporated into a two-step process to efficiently form Rydberg states of Ps, with potential applications in synthesis of cold antihydrogen, gravity measurements with antimatter, or for injection of electrons and positrons into a stellarator.

Keywords: antimatter, positronium, Doppler spectroscopy, nonlinear optics

1. Introduction

The positronium (Ps) atom—the bound-state of an electron and a positron—has long been of interest for its unique spectroscopic properties [1]. Hydrogen-like in its simplicity and purely leptonic, Ps is a suitable candidate for precision tests of bound-state QED [2–5]. It has also been highlighted as a part antimatter probe for testing the weak equivalence principle of general relativity [6], and as a component in efficient schemes for synthesis of antihydrogen [7–9].

The gross energy levels of Ps can be found by analogy with the Bohr model for hydrogen, scaling with the inverse-square of the principal quantum number, although with half the binding-energy of H, i.e. $E_n = 6.8/n^2$ (eV). A range of experiments which aim to harness the extraordinary properties of Ps require Rydberg states ($n \gtrsim 10$) (e.g. [6, 7, 10–12]), not least because the lifetime against the mutual annihilation of the constituent particles is significantly increased. Also, Rydberg states of Ps can have very large effective electric dipole moments [12], which could be exploited to manipulate —or even trap—the atoms, using inhomogeneous electric fields [13]. Furthermore, the cross-section for the formation of antihydrogen by mixture of antiprotons with Ps scales classically like $\mathcal{O}(n^4)$.

Two-step, laser-excitation of Ps from the ground-state via $n = 2$ to $n = 10$–15 has been demonstrated previously as a means to attain Rydberg states [14, 15], with recent refinements [16] resolving states as high as $n = 31$. In every case, the first step, from the ground-state to $n = 2$, was achieved as a single-photon transition (i.e. 1S–2P) using an ultraviolet laser tuned to resonance ($\lambda_0 = 243$ nm). Efficient laser-excitation is

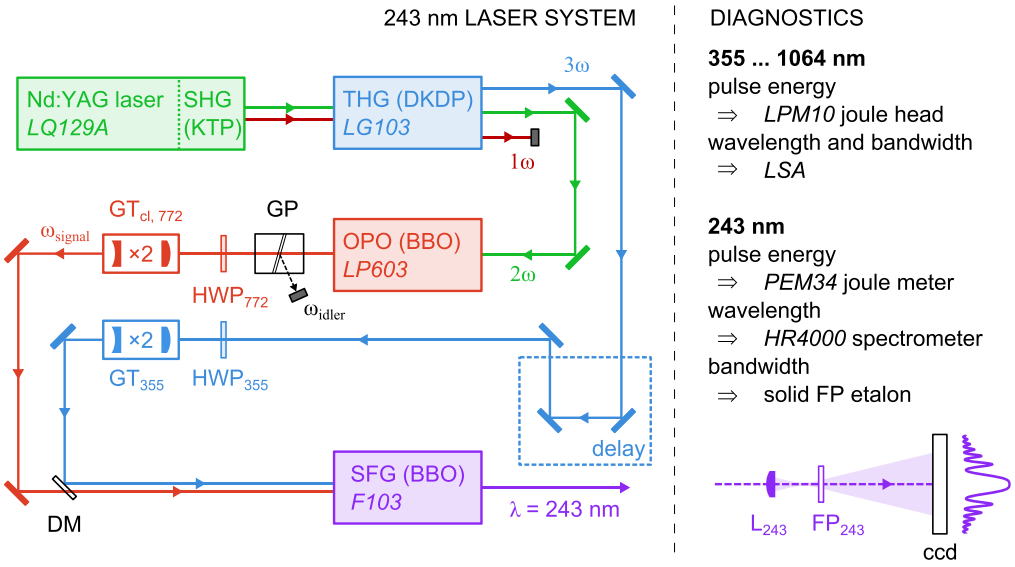

Figure 1. Schematic depiction of the broadband laser source utilized for Ps excitation at $\lambda = 243$ nm. GP = Glan polarizer; HWP = half-wave plate; $GT_{(CL)}$ = Galilean telescope (with cylindrical lenses); DM = dichroic mirror; L = plano-convex lens; FP = solid Fabry–Perot etalon. Numbers in subscript indicate the associated laser wavelength in nm. For further details see text.

hampered by the extremely broad Doppler-width associated with typical Ps sources, which arises as a consequence of the element's uniquely low rest-mass. The Doppler broadened 1S–2P linewidth of a room temperature (300 K) distribution is on the order of THz: far exceeding the linewidth of the majority of commercial laser systems (typically <10 GHz), and thus only some fraction of the Ps within an ambient ensemble could be excited into Rydberg states using such. In the aforementioned Ps spectroscopy works Ziock *et al* [14]/Cassidy *et al* [15] used modified, pulsed dye lasers, with bandwidths of about 350/135 GHz, and pulse energies of about 0.3/1.0 mJ at $\lambda = 243$ nm. The fairly rapid deterioration of the laser dyes is unavoidable, and introduces inconsistency to prolonged measurement periods (for e.g. precision spectroscopy). Accordingly, such lasers require regular dye changes and expert attention, which in some cases is impractical and motivates pursuit of alternative schemes (e.g. [17]).

In this article we describe and characterize a broadband ($\Delta\nu \approx 225$ GHz), tunable, solid-state UV laser ($\lambda = 243$ nm), with a 1.2 mJ output in an 8 ns pulse. In contrast to the discussed pulsed dye laser systems, our employment of purely solid-state, nonlinear processes ensures a reliable laser output over many months, and the high peak intensity and broad bandwidth are well suited to efficiently driving the Doppler broadened Lyman-α transition of Ps. We demonstrate use of this laser in exciting ground-state Ps atoms, with a view to pursuing subsequent excitation from $n = 2$ into Rydberg states.

2. Experimental details

2.1. A tunable, broadband, UV laser source

The laser source which produces the $\lambda = 243$ nm radiation for the $1^3S \rightarrow 2^3P$ transition of Ps is an all-solid-state system. The UV light is generated using nonlinear optics, by the sum-frequency of the third harmonic of an Nd:YAG laser (3ω, $\lambda = 355$ nm) and the signal-wave of an infra-red, tunable optical parametric oscillator (OPO) (ω_s, $\lambda = 772$ nm). The configuration of this UV laser source is depicted schematically in figure 1.

The Q-switched Nd:YAG laser (SOLAR LQ129A) nominally operates at 10 Hz and is based on a stable ring cavity, with a smooth 2D Gaussian output beam profile and total beam diameter of approximately 8 mm. It provides laser radiation at its fundamental wavelength of $\lambda = 1064$ nm in a pulse of width of ~12 ns (FWHM), with an output energy per pulse of 420 mJ. A temperature stabilized KTP nonlinear crystal within the laser unit generates the second harmonic ($\lambda = 532$ nm), with a pulse energy of 220 mJ. These infra-red and visible beams exit the laser unit co-linearly.

The 1ω and 2ω waves were mixed in an harmonic generator (SOLAR LG103), which is based on a temperature stabilized DKDP nonlinear crystal. The $\lambda = 355$ nm, third-harmonic wave generated in the crystal could be tuned to produce up to 60 mJ in a 10 ns pulse. The three harmonics, at 1064, 532 and 355 nm, were separated using two dichroic mirrors.

The remaining 2ω radiation was used to pump a pair of BBO nonlinear crystals, which were held in the $L_c = 11$ cm cavity of an OPO (SOLAR LP603). The OPO cavity is singly-resonant, exhibiting an approximate TEM_{01} transverse mode beam profile. Only the signal-wave generated by the OPO was utilized in these experiments; this was separated from the orthogonally polarized, longer wavelength idler-wave and remaining pump using a polarizing beam splitter. Wavelength selection was achieved by angular phase-matching of the BBO crystals. Tuned for a wavelength of

Table 1. Operating data for the components within the 243 nm laser source. The spectral information was obtained by use of an *High Finesse* LSA, except where indicated otherwise. The uncertainty in the energy per pulse is due to shot-to-shot fluctuations.

Laser source	λ (nm)	$\Delta\lambda$ (nm)	$\Delta\nu$ (GHz)	Δt (ns)	E_{pulse} (mJ)
Nd:YAG LQ129A	1064.501	0.113	30 ± 1	12 ± 1	490 ± 5
	532.246	0.031	32 ± 2	12 ± 1	260 ± 5
+ LG103	355.831	0.026	61 ± 2	10 ± 1	40 ± 2
OPO LP604	772.448	0.325	163 ± 3	9 ± 1	25 ± 2
SFG[a]	243.152	0.044	225 ± 3	8 ± 1	1.2 ± 0.3

[a] Linewidth measured using a solid etalon interferometer—see text.

$\lambda \sim 770$ nm, energies up to 37 mJ could be achieved in an 8 ns pulse, however, when optimized for subsequent UV production this reduced to ~25 mJ.

A cylindrical Galilean telescope was employed to correct the horizontal divergence of the OPO signal-wave, which was then guided to a dichroic mirror that overlaid the pulse with the third-harmonic of the Nd:YAG. Prior to their mixing, the profile of the latter was ×2 compressed with a Galilean telescope, and its path length arranged such that the peak power of the pulse had near-perfect temporal overlap (<1 ns) with the OPO signal-wave at the point where the two combine.

With approximately matching beam diameters (~5 mm), the OPO signal-wave and Nd:YAG third-harmonic were steered to a sum-frequency generator (SFG, SOLAR F103), which held an appropriately AR coated, 7 mm long BBO nonlinear crystal. Fine adjustment to the phase-matching of the Nd:YAG harmonic production was used to roughly equate the number of photons in the 770 and 355 nm beams, thereby optimizing the sum-frequency generation of the $\lambda = 243$ nm UV pulse yielded by the SFG, which was isolated from the two pump beams using a series of dichroic mirrors. The UV beam was steered to the Ps interaction region (section 2.2); entering and exiting the vacuum system via uncoated, CaF_2 windows. An HR coated mirror outside of the system was used to reflect the laser back through for a second pass of the Ps cloud (see figure 3).

Each laser pulse (Nd:YAG 1ω, 2ω and 3ω; OPO signal-wave; 243 nm pulse) has been characterized for pulse energy (E_{pulse}), time-width (Δt), wavelength (λ) and linewidth ($\Delta\nu$)—these are summarized in table 1. The pulse energies were measured using joule meter heads (Coherent LMP10 for pulse energies >5 mJ, Sensor und Lasertechnik PEM-34 for lower pulse energies), and the time-widths using a high-speed, fibre-coupled Si photodiode (Thorlabs SV2-FC). The spectral characteristics for the Nd:YAG and OPO waves were measured using a laser spectrum analyser (High Finesse, LSA), which has an operating wavelength range of 350–1120 nm, frequency accuracy of ~6 GHz and a FWHM range of 3–2000 GHz. The UV wavelength was determined using an Ocean Optics HR4000, which is optimized for 220–260 nm, having a resolution of $\Delta\lambda = 0.052$ nm at $\lambda = 240$ nm (this device was calibrated against UV emission lines from palladium and cobalt hollow cathode lamps: Heraeus 3QNYPd and 3QNYCo). The LSA and HR4000 respectively lack the range and resolution to measure the linewidth of the 243 nm pulse; accordingly, an etalon-based UV spectrometer was constructed.

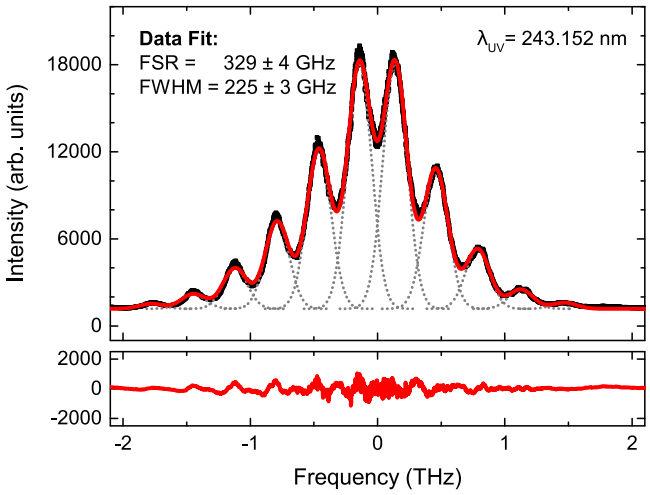

Figure 2. Typical etalon fringe pattern recorded using a CCD line array detector, averaged over 300 laser pulses (black points). The red line represents a fit to the data of the sum of equal-width Gaussians (grey dots); the fit residuals are plotted below.

The set up for the characterization of the UV pulse linewidth is included in figure 1, and in essence it comprises a cylindrical lens and very high-finesse, thin, solid etalon (Laser Optik GmbH, 0.2 mm thick substrate ET-S-00185 with HR-coating B-10204), through each of which the UV pulse was passed. The resulting fringe pattern was imaged by a line CCD camera (Alphalas GmbH, CCD-S3600-D-UV). The etalon has a free spectral range of 330 GHz and the specified reflectivity $R > 0.995$ at 243 nm translates into a theoretical finesse of $\mathcal{F} > 600$.

A typical trace of the fringes imaged by the CCD is shown in figure 2. The fringe pattern was fitted using the sum of equal width Gaussians, and was found to reproduce the fringe spacing expected from the etalon specifications. The value of FWHM = 225 ± 3 GHz determined from the pattern fit approximately agrees with the convolution of the widths of the 355 and 770 nm beams (~190 GHz), and indicates that the UV laser continuously covers a significant fraction of the Doppler broadened linewidth for a 300 K thermal distribution of Ps atoms.

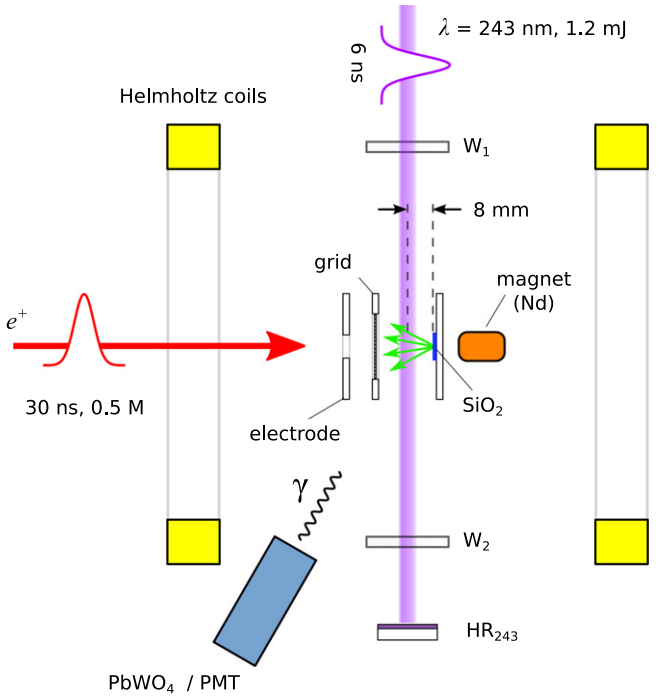

Figure 3. Schematic illustration of the positronium (Ps) converter assembly and the UV laser interaction path (purple). The red arrow marks the path of the positrons from the accumulator and the green arrows represent Ps emitted from the porous silica film.
HC = Helmholtz coils; W_i = CaF_2 UV windows; HR_{243} = UV reflector; PMT = photo-multiplier tube.

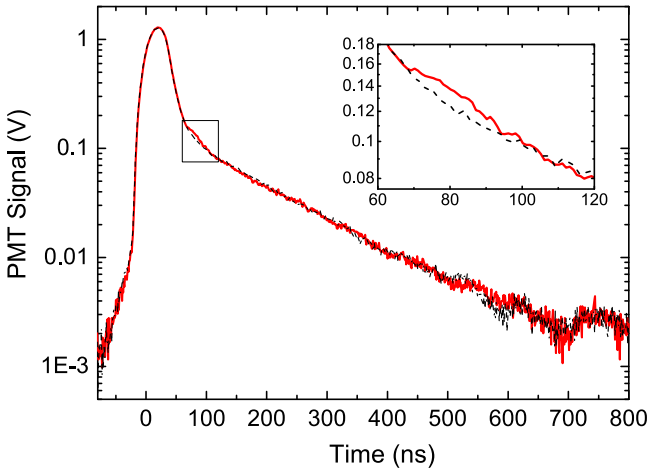

Figure 4. Example SSPALS signal recorded from the $PbWO_4$/PMT detector, i.e. time-resolved, annihilation γ-ray flux as a 30 ns bunch of positrons is implanted into mesoporous silica (averaged from 100 repeat measurements). The delayed events are due to annihilation of free o-Ps. The solid line is the trace recorded with the $\lambda = 243$ nm beam passing through the Ps cloud at $t \approx 80$ ns (zoom inset), in contrast to a background measurement with no laser (dashed).

2.2. Ps production

Positrons emitted via β^+ decay from a 1.25 GBq sample of the radioisotope ^{22}Na were moderated to energies of a few eV using a thin layer of solid neon [18]. These were then guided in vacuum using magnetic fields to a buffer-gas positron accumulator [19] that consists of two stages of cylindrical electrodes lying parallel to the 35 mT field of an encasing solenoid—see [20] for further details. Inelastic collisions between impinging positrons and low density molecular nitrogen gas resulted in capture of the positrons, which subsequently cool to the axial minimum of an electric potential formed by appropriately biasing the electrodes. A rotating dipole electric field applied across the cloud (known as the 'rotating-wall', RW, technique [21, 22]) reduced positron losses due to diffusion to the electrode walls, and radially compressed the cloud to $\sigma_{e^+} \approx 1$ mm (2D Gaussian areal profile) [23–26]; a low pressure cooling gas (SF_6) was employed to counteract heating of the cloud by the rotating field.

The positrons were released from the trap by asymmetrically lowering the trapping potential, ejecting a pulse of roughly 5×10^5 particles at a repetition rate of 0.3 Hz. These would drift 1.5 m along the magnetic field lines generated by a series of coils to the Ps converter assembly (figure 3), and there pass through the centre of an alignment electrode and then a tungsten grid. An electric field applied between the grid and target mount accelerated the positrons to embed them into the surface of a porous silica film. This 400 mm^2 mesostructured film was grown using Pluronic F-127 ethyleneoxide/propyleneoxide block copolymer (BASF), with 0.016 F-127/Si molar ratio, and deposited 700 nm thick on to a silicon substrate [27]. The positrons were implanted into the film with a time-width (FWHM) of roughly 30 ns.

The embedded positrons rapidly (<1 ns) cool via collisions inside the insulator bulk [28], and in so-doing may capture electrons to form Ps. These Ps atoms then diffuse and likely become captured by the pore structure, wherein they may survive for some significant fraction of their lifetime in vacuum [29]. The vacuum lifetime is determined by the total spin of the particle/ antiparticle pair and in the ground-state: the $s = 0$ singlet (para-Ps) has a mean lifetime of 0.12 ns; whereas the $s = 1$ triplet state (ortho-Ps) has a mean lifetime of 142 ns. The pores interlink and provide channels to the sample surface, facilitating emission to vacuum of the longer lived o-Ps atoms with reasonable efficiency (~0.3 /e^+) [30].

The production of free o-Ps was inferred using the technique of 'single-shot positron annihilation lifetime spectroscopy' (SSPALS) [31], performed using a fast, lead-tungstate ($PbWO_4$) scintillator and a PMT detector. The $PbWO_4$ crystal is cylindrical in geometry, measuring 50 mm in diameter and 40 mm long. The high density material exhibits excellent γ-ray absorption and the scintillation decay time is sufficiently fast (~9 ns) that the rapid annihilation of positrons and p-Ps following positron implantation, can be resolved from the delayed annihilation of o-Ps emitted to vacuum. Two example SSPALS traces are plotted in figure 4.

The o-Ps lifetime was estimated by fitting the decay component of the delayed fraction of the SSPALS spectra, giving $\tau \approx 120$ ns [32]. This is somewhat shorter than the free o-Ps vacuum lifetime (142 ns), and is likely distorted by other phenomena neglected by the fitting model, e.g. Ps trapped in isolated pores ($\tau \approx 74$ ns, [30]) and transport of the fastest atoms away from the detector. Furthermore, a permanent

magnet (Nd) placed behind the target was used to increase the magnetic field in the interaction region to ∼75 mT, which will have caused Zeeman mixing of the p-Ps and o-Ps states with the same magnetic quantum number [33–36]; this magnetic quenching is estimated to have reduced the mean lifetime of ground-state o-Ps to approximately 135 ns.

3. Results and discussion

3.1. Ps spectroscopy

SSPALS measurements were conducted with the UV laser pulse (section 2.1) triggered to pass through the interaction region shortly after the Ps atoms were formed (∼80 ns). Tuned to resonance ($\lambda_0 = 243.02$ nm), the laser would be expected to efficiently drive $1^3S_1 \rightarrow 2^3P_J$ transitions (where $J = 0, 1, 2$); we assume states of 1^1S_0 are negligible, due to its rapid rate of self-annihilation. In a vacuum environment free from electromagnetic fields, 2P states of ortho-Ps are quasi-stable against direct annihilation [37]. The radiative decay back to the ground-state is comparatively rapid (3.2 ns), therefore Ps atoms excited to the 2P states would most likely annihilate following such decay and the overall average lifetime compared to atoms that are not excited would be only marginally increased. Such a small difference in lifetime would be difficult for us to identify using SSPALS. However, in the first excited state the hyperfine interval is much less than that of the ground-state [2], therefore exciting Ps to $n = 2$ in the field of the nearby permanent magnet (figure 3) significantly enhances the Zeeman mixing between the triplet and singlet states. Prompt annihilation following radiative decay to the p-Ps ground-state (see figure 5) will result in a near immediate excess of γ-rays evident in the lifetime spectra, relative to the case in which excitation does not take place.

The annihilation 'excess' due to excitation + magnetic quenching was quantified by taking the fraction of the total signal of the SSPALS spectra as measured in a 10 ns window coincident with the applied laser (see figure 4, inset), and finding the relative difference in signal compared to a background measurement for which the UV laser was de-tuned far from resonance. Figure 6 shows how this parameter varies as the laser is tuned across the Doppler profile of the Lyman-α transition, for a range of voltages applied to the target mount, indicating a clear resonance centred at 243 nm.

For the time-width and beam profile of the laser system described in this work, the saturation intensity of the 1S–2P transition corresponds to a pulse energy of around 3.5 μJ. Experiments have found significantly higher than expected intensities are in fact required (equivalent to ∼200 μJ per pulse) [33, 36], nonetheless the measured 1.2 mJ is likely to saturate all of the Ps atoms inside the laser-field. However, it is clear from figure 4 that only a small fraction of the o-Ps atoms are ultimately magnetically quenched—we estimate approximately 1%. This is much less than the ∼35% that are thought to fall within the laser bandwidth (assuming a room temperature distribution). This is partly because only a subset

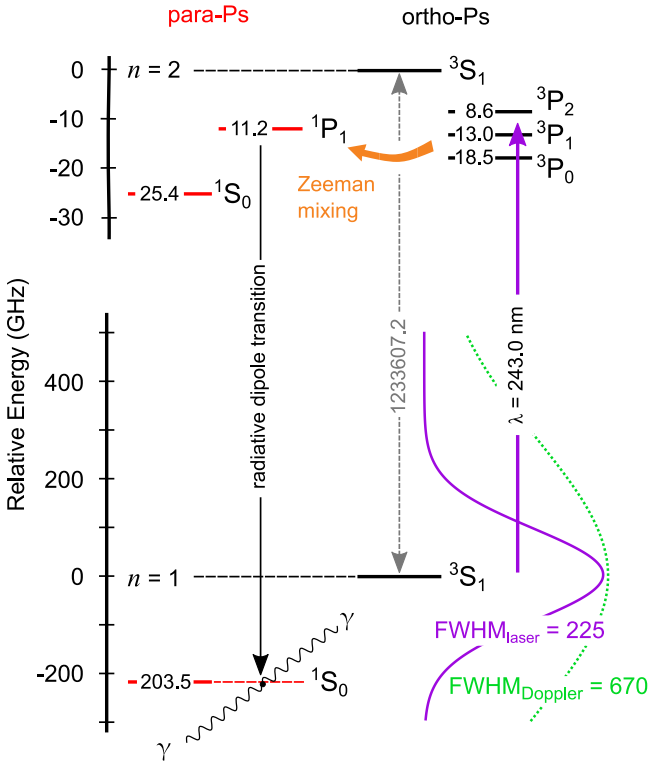

Figure 5. Ps energy level scheme, 1S–2P dipole transition and width functions; note the difference in energy scale for $n = 2$. The radiative lifetime from 2P to the ground-state is 3.2 ns. For further details see text.

of the 2P triplet states can magnetically mix with the singlet states that we detect; in addition to which the extent of any mixing will vary with the position of the atoms in the inhomogeneous magnetic field of the permanent magnet. Moreover, the laser pulse is short in comparison to the time-width of the positron bunch, and the position of the interaction region is sufficiently far from the surface of the film that both annihilation during transport and dispersion of the Ps atoms will markedly reduce the number of atoms the laser can address. Optimization of the geometry of the set-up, combined with time-focusing of the positron bunch, should improve this significantly. Furthermore, switching to a detection scheme based upon resonance-enhanced multi-photon ionization (REMPI) [38] (insensitive to the 2P sub-states), would further strengthen the potential signal.

3.2. Ps cooling

The positrons were implanted into the silica film with energy K, as determined by the electric bias that attracts them to the target. The positron stopping profile within the film is expected to follow a Makhovian distribution [21], giving a mean depth at which Ps forms $\propto K^{\nu}$ (where ν is material dependent and estimated to be ∼1.6 for silica [28]). Following formation, Ps may be ejected from the bulk into the porous network with an energy of ∼1 eV [39]. Subsequent collisions with the inner surface of the pores will cool the atoms as they diffuse to the surface. Those formed deeper (i.e., higher target bias) will, on average, spend longer inside the pores and thus

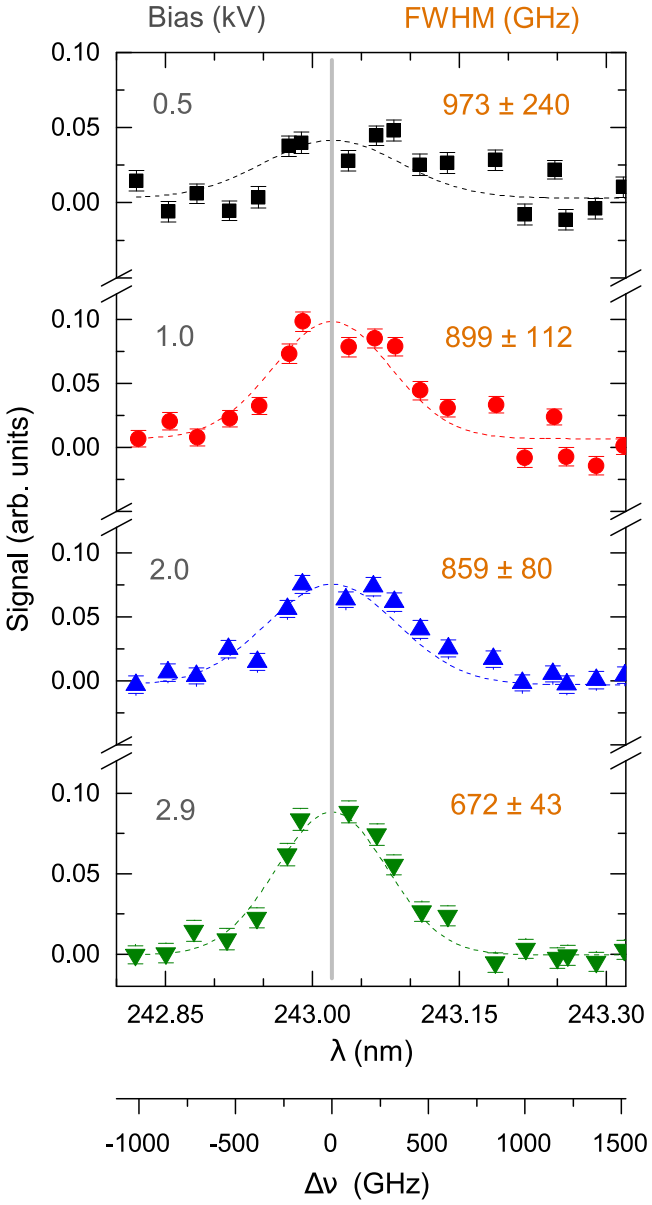

Figure 6. The excess SSPALS signal (during the excitation window), as a function of the UV laser wavelength and target bias, averaged over 300 laser pulses. The SSPALS data are normalized to represent a relative increase with respect to the laser-off-resonance signal. The dashed lines represent Gaussian fits to the data.

be emitted to vacuum with less energy than Ps formed nearer the surface. This is evident in the narrowing of the Doppler profiles of figure 6, in accordance with previous studies [30, 36].

The 1S–2P line profiles plotted in figure 6 were fitted with Gaussian functions, then the Doppler-width found by deconvolution of the width of those fits with that of the UV laser. The root-mean squared (rms) velocity of the Ps atoms in the direction of the laser $\langle v_x^2 \rangle$ was determined by assuming non-relativistic Doppler broadening, i.e. $\langle v_x^2 \rangle = (c\sigma/\lambda_0)^2$, where c is the speed of light and σ is the deconvolved width of the Gaussian fit. The kinetic energy associated with the rms velocity, $\langle E_x \rangle = \frac{1}{2} m_{\mathrm{Ps}} \langle v_x^2 \rangle$, is plotted against the target bias in figure 7.

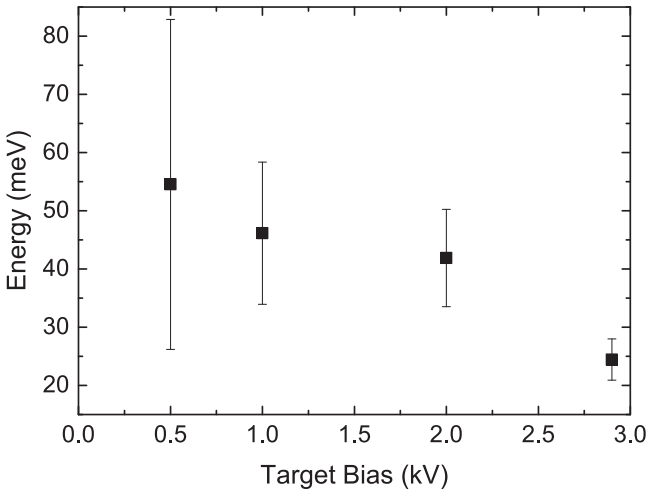

Figure 7. The kinetic energy associated with the rms velocity of positronium emitted from mesoporous silica, as measured by Doppler broadened laser spectroscopy of the 1S–2P transition. See text for details.

For arbitrarily large pores Ps atoms would eventually thermalize with the 300 K silica bulk, for which we would expect to measure $\langle E_x \rangle \approx 25$ meV. However, if the pores are very small the ground-state of the pore/atom system can exceed the thermal energy of the bulk, effectively raising the minimum emission energy of the Ps atoms—e.g. for Ps in a spherical infinite square potential $E_0 = \hbar^2\pi^2/m_e d^2 \approx 25$ meV ($d = 5.5$ nm). As shown in figure 7, the minimum Ps energy measured was 24 ± 3 meV. This suggests that the pores are no smaller than the 5 nm diameter expected for F-127 films.

Time-of-flight experiments have previously measured energies of 48 ± 5 meV for Ps emitted from similar films [30]. It is important to note that those measurements relate to the centre-of-mass motion of Ps in the direction perpendicular to the film's surface, whereas we report energies associated with the velocity distribution along the direction of propagation of the UV laser, parallel to the silica film, and the two—although related—are not equivalent. The emission properties which dictate the relationship between the two measurements are complicated by unknown details of the film, such as the homogeneity of the pore size and the (an)isotropy of its structure, in particular at the surface. Assuming uniformity in pore size, emission of Ps cooled to the ground-state of the pore should be almost mono-energetic, and the distribution of velocities along a particular axis would arise as a consequence of the angular distribution of the emission.

A similarly conducted Doppler-width measurement by Cassidy *et al* reported Ps energies of 41.7 ± 2.7 meV [36], however the authors used films known to have smaller pores ($d \approx 2.7$ nm), which are expected to emit Ps with higher energies. It is important to note that the technique of probing the Ps atoms with pulsed lasers likely only samples a subset of the distribution (as already discussed in section 3.1), and that varying the timing, location and size of the laser can conceivably affect the measured Doppler-width. For instance,

the experiments discussed here were performed with the laser positioned 8 mm from the film. Assuming a mono-energetic beam moving at 10^5 ms^{-1}, the forward directed atoms will arrive at the interaction region in around 80 ns, whereas those emitted at larger angles will naturally take longer and hence the number of these measured will be lessened due to increased self-annihilation en route, effectively narrowing the measured distribution; what's more those atoms with high emission angles are more likely to miss the interaction region altogether, further narrowing the measured width. Conversely, if the laser were triggered too early, such that only the fastest, non-thermalized Ps can reach the interaction region when the laser fires, a broader Doppler-width might be measured.

4. Concluding remarks

The tunable UV laser described in section 2.1 has been demonstrated in exciting ground-state Ps to the 2P state. The measured characteristics of this $\lambda = 243$ nm laser, in particular the bandwidth ($\Delta\nu = 225$ GHz) and pulse energy ($E_{\text{pulse}} = 1.2$ mJ), find it well matched for saturating a large fraction of presently achievable, pulsed Ps sources. Furthermore, unlike previous 1S–2P laser-spectroscopy studies of Ps that all utilized dye lasers [33, 36], the solid-state system is extremely stable and requires minimal maintenance.

The measurement of the 1S–2P Doppler-width made using this laser ($\Delta\nu = 672 \pm 43$ GHz) is in reasonable agreement with previous works that used nominally identical Ps production techniques, however further refinement to the experimental set-up could significantly improve the signal and statistics. For instance, bunching of the positron clouds using time-varying electric fields is relatively straightforward [40] and can achieve time-widths in the region of 1 ns, which would dramatically improve the fraction of the subsequently formed Ps distribution that the laser can address. Modification to the target system in conjunction with optimization of the UV beam profile would enable positioning of the interaction region far closer to the surface of the film (<1 mm), improving the overlap further and exciting the atoms before self-annihilation and dispersion become significant.

As the signal induced by magnetic quenching was used in these measurements it is difficult to determine exactly how efficiently the $n = 2$ state was populated—especially as the magnetic field in the interaction region was inhomogeneous. Also, detection of magnetically-quenched states is less efficient than would be that of the ionization of excited atoms, e.g. by use of a second laser pulse (REMPI), as then all substates of the 2P manifold can contribute to the signal. To resonantly photoionize the excited Ps atoms would require an near infra-red laser $\lambda = 729$ nm; it is convenient to instead use the $\lambda = 532$ nm second harmonic of a Nd:YAG [41], although the cross-section is smaller and a higher intensity is needed to saturate the transition into the continuum ($\sim 10^{11}$ W m^{-2}). Ideally we would instead detect excitation/ionization events directly, e.g. using a micro-channel plate detector, with the potential to drastically improve the signal-to-noise ratio compared to lifetime measurements. This is more viable when studying Rydberg states, as the atoms become so long-lived they are able to drift to a distinct detection region [16].

The prospect of efficient production of long-lived, excited states of Ps atoms via a 1S–2P-nD/nS laser excitation scheme has a number of exciting applications, but is contingent upon maximizing population of the first excited state, as discussed in this work. A number of relatively simple improvements (see above) are expected to garner marked progress towards this goal, with applications in experiments ranging from gravity measurements with antihydrogen [10] or Ps [12], to study of electron/positron plasmas in a stellarator [11]. Even the present proof-of-concept state of the experimental configuration has the proven ability to measure the 1S–2P Doppler-width, which could be exploited as a means to evaluate new materials and technologies designed for production of ever colder Ps atoms that are likely a prerequisite to attainment of the long-anticipated Ps Bose–Einstein condensate [42].

Acknowledgments

We thank the EPSRC for its support, currently via award EP/L014718/1 and for studentship funding for AD, TM and DE. DPvdW thanks the Leverhulme Trust for Research Fellowship award RF-2012-495. We acknowledge the work of S J Kerrigan, C J Baker, R J Lewis, P R Watkeys, D C S Beddows, J Clarke, and B C Griffiths in preliminary development of both the laser system and positron beam. We also thank D B Cassidy for numerous helpful discussions. The authors are grateful to L Liszkay for providing the silica films, and to J Kivell, P Hopkins and H Thomas for their enthusiastic technical support.

References

[1] Ruark A E 1945 *Phys. Rev.* **68** 278
[2] Ley R 2002 *Appl. Surf. Sci.* **194** 301 IX International Workshop on Slow Positron Beam Techniques for Solids and Surfaces
[3] Berko S and Pendleton H N 1980 *Ann. Rev. Nucl. Part. Sci.* **30** 543
[4] Rich A 1981 *Rev. Mod. Phys.* **53** 127
[5] Karshenboim S G 2004 *Int. J. Mod. Phys.* A **19** 3879
[6] Mills A P Jr and Leventhal M 2002 *Nucl. Instrum. Meth.* B **192** 102
[7] Charlton M 1990 *Phys. Lett.* A **143** 143
[8] Deutch B I, Charlton M, Holzscheiter M H, Hvelplund P, Jørgensen L V, Knudsen H, Laricchia G, Merrison J P and Poulsen M R 1993 *Hyperfine Interact.* **76** 151
[9] Storry C H *et al* 2004 *Phys. Rev. Lett.* **93** 263401
[10] Kellerbauer A *et al* 2008 *Nucl. Instrum. Meth.* B **266** 351–6 proceedings of the XIV International Workshop on Low Energy Positron and Positronium Physics
[11] Sunn Pedersen T, Danielson J R, Hugenschmidt C, Marx G, Sarasola X, Schauer F, Schweikhard L, Surko C M and Winkler E 2012 *New J. Phys.* **14** 035010

[12] Cassidy D B and Hogan S D 2014 *Int. J. Mod. Phys. Conf. Ser.* **30** 1460259
[13] Wing W H 1980 *Phys. Rev. Lett.* **45** 631
[14] Ziock K P, Howell R H, Magnotta F, Failor R A and Jones K M 1990 *Phys. Rev. Lett.* **64** 2366
[15] Cassidy D B, Hisakado T H, Tom H W K and Mills A P Jr 2012 *Phys. Rev. Lett.* **108** 043401
[16] Jones A C L, Hisakado T H, Goldman H J, Tom H W K, Mills A P Jr and Cassidy D B 2014 *Phys. Rev.* A **90** 012503
[17] Cialdi S, Boscolo I, Castelli F, Villa F, Ferrari G and Giammarchi M 2011 *Nucl. Instrum. Meth.* B **269** 1527
[18] Mills A P Jr and Gullikson E M 1986 *Appl. Phys. Lett.* **49** 1121
[19] Murphy T J and Surko C M 1992 *Phys. Rev.* A **46** 5696
[20] Clarke J, van der Werf D P, Griffiths B, Beddows D C S, Charlton M, Telle H H and Watkeys P R 2006 *Rev. Sci. Instrum.* **77** 063302
[21] Huang X P, Anderegg F, Hollmann E M, Driscoll C F and O'Neil T M 1997 *Phys. Rev. Lett.* **78** 875
[22] Greaves R G and Surko C M 2000 *Phys. Rev. Lett.* **85** 1883
[23] Isaac C A, Baker C J, Mortensen T, van der Werf D P and Charlton M 2011 *Phys. Rev. Lett.* **107** 033201
[24] van der Werf D P, Isaac C A, Baker C J, Mortensen T, Kerrigan S J and Charlton M 2012 *New J. Phys.* **14** 075022
[25] Isaac C A 2013 *Phys. Rev.* A **87** 043415
[26] Deller A, Mortensen T, Isaac C A, van der Werf D P and Charlton M 2014 *New J. Phys.* **16** 073028
[27] Liszkay L *et al* 2008 *Appl. Phys. Lett.* **92** 063114
[28] Schultz P J and Lynn K G 1988 *Rev. Mod. Phys.* **60** 701
[29] Wada K and Hyodo T 2013 *J. Phys.: Conf. Ser.* **443** 012003
[30] Crivelli P, Gendotti U, Rubbia A, Liszkay L, Pérez P and Corbel C 2010 *Phys. Rev.* A **81** 052703
[31] Cassidy D B, Deng S H M, Tanaka H K M and Mills A P Jr 2006 *Appl. Phys. Lett.* **88** 194105
[32] Deller A 2013 Positron Accumulation and Laser Excitation of the Positronium Atom *Ph.D. thesis* Swansea University
[33] Ziock K P, Dermer C D, Howell R H, Magnotta F and Jones K M 1990 *J. Phys. B: At. Mol. Opt.* **23** 329
[34] Curry S M 1973 *Phys. Rev.* A **7** 447
[35] Dermer C D and Weisheit J C 1989 *Phys. Rev.* A **40** 5526
[36] Cassidy D B, Crivelli P, Hisakado T H, Liszkay L, Meligne V E, Pérez P, Tom H W K and Mills A P Jr 2010 *Phys. Rev.* A **81** 012715
[37] Alekseev A 1958 *Sov. Phys. JETP* **34** 826
[38] Demtröder W 2003 *Laser Spectroscopy* 3rd ed (New York: Springer) ISBN 3-540-65225-6
[39] Nagashima Y, Morinaka Y, Kurihara T, Nagai Y, Hyodo T, Shidara T and Nakahara K 1998 *Phys. Rev.* B **58** 12676
[40] Mills A P Jr 1980 *Appl. Phys.* **22** 273
[41] Cassidy D B, Hisakado T H, Tom H W K and Mills A P Jr 2012 *Phys. Rev. Lett.* **109** 073401
[42] Platzman P M and Mills A P Jr 1994 *Phys. Rev. B* **49** 454